Interlaced scanning by laser ultrasonic for defects imaging of train rail surface

Yuehong Zhang, Lin Luo, Yu Zhang, Xiaorong Gao, Jiang Long

Yuehong Zhang, Lin Luo, Yu Zhang, Xiaorong Gao, Jiang Long, "Interlaced scanning by laser ultrasonic for defects imaging of train rail surface," Proc. SPIE 11209, Eleventh International Conference on Information Optics and Photonics (CIOP 2019), 112091L (20 December 2019); doi: 10.1117/12.2547455

SPIE.

Event: Eleventh International Conference on Information Optics and Photonics (CIOP 2019), 2019, Xi'an, China

Interlaced scanning by laser ultrasonic for defects imaging of train rail surface

Yuehong Zhang[a],Lin Luo[a] ,Yu Zhang*[a],Xiaorong Gao[a] ,Jiang Long[a]
[a]School of Physical Science and Technology, Southwest Jiaotong University, Chengdu 610031, China

ABSTRACT

In this paper, the technique of laser ultrasonic rapid detection of rail surface defects is studied, the interlaced laser ultrasonic defect detection imaging scheme is designed: the laser ultrasonic signal is excited and detected on both sides of the rail, the image is fusion-registered by algorithms such as filtering and image registration to obtain a complete rail surface inspection image to display defect characteristics, which solves the problem that laser ultrasonic is not sensitive to defects. According to the theory of thermal bomb and the proposed detection scheme, a finite element model is established to simulate the propagation process of laser ultrasonic signals in the rail, and the detection signal with surface defects information is obtained. In order to verify the effectiveness of the proposed method, a series of experiments were carried out to obtain the rail detection image with surface defects, and the influence of the laser spot size on the detection image results was analyzed. The experimental results show that the proposed laser ultrasonic imaging detection method can quickly obtain the detected image and effectively display the defect characteristics. The laser spot size has a significant influence on the detection result. When the laser spot is small, the effect of the detection image can be improved. The proposed method provides a reference for further establishing the actual rail inspection system.

Keywords: Laser ultrasound imaging, train rail, NDT, finite element analysis

1. INTRODUCTION

Safety and reliability are two key issues in the railway field. Rails, which are often the main cause of failures and accidents, are most susceptible to static stress or fatigue, especially when the rail is overloaded by rail and wheel contact[1], which can result in many different types of defects[2]. Laser ultrasonic technology is a new ultrasonic detection method. It not only has the advantages of conventional ultrasound, but also has the characteristics of rich wave mode, high precision and frequency bandwidth, which has attracted wide attention in the industry[3]. Therefore, the use of laser ultrasonic technology to detect rail defects has important theoretical significance and research value.

In the early days of studying laser ultrasound technology, scholars theoretically used the eigenfunction method[4] and the Green's function method[5] to solve equations to study the relationship between laser excitation and ultrasonic propagation, but the eigenfunction method is only suitable for solving thin materials. Because the theoretical solution to the equation is complicated and cumbersome, the analytical model becomes difficult to process for complex geometries or defective specimens. Therefore, the finite element method is used to study laser ultrasound[6, 7]. The finite element method can not only simulate the branched surface-breaking defects[8], but also simulate that the ultrasonic guided wave detects microcracks in model[9]. Laser-ultrasonics has been applied in different fields for defects detection, in the aeronautical field for damage detection on thick composite materials[10] and honeycombs[11], in the railway field for rail[12, 13], rail wheels[14] and axle[15] inspection and in metal slabs production. In the existing ultrasonic technology, there is a disadvantage that the probe needs to be in contact with the object to be investigated, which lengthens the inspection time necessary to prepare the object and apply the coupling medium. Therefore, in recent years, domestic and foreign scholars have combined laser ultrasonic technology with air coupling technology to detect defects in train wheels[16] and axles[17]. The system can adapt well to the profile of the tested specimens and has strong adaptability. For the laser ultrasonic technology, not only the detection object is studied, but also the laser parameters[18] and laser light source[19, 20] are studied in detail, which greatly improves the detection ability of the laser ultrasonic detection technology for the internal crack of the metal.

* zhang.yuer@163.com; phone 136 8348 0269

Eleventh International Conference on Information Optics and Photonics (CIOP 2019)
edited by Hannan Wang, Proc. of SPIE Vol. 11209, 112091L · © 2019 SPIE
CCC code: 0277-786X/19/$21 · doi: 10.1117/12.2547455

In this paper, the three-dimensional rail finite element model with surface defects is established, and the effect of rapid detection of defects is achieved by using interlaced imaging technology, which provides a basis for further research in the future. The structure of this paper is as follows: the principle of interlaced imaging and the theoretical basis of finite element method are introduced in Section 2. A laser interlaced imaging scheme is designed to determine the position of the laser excitation and reception signals and determine the size of the grid and time step to obtain the best signal-to-noise ratio ultrasonic signal. The interlaced imaging method is used to obtain the rail detection image with surface defects, and it is verified that the laser spot size affects the effect of detecting the image in Section 3.

2. METHODOLOGY

In this section, the coupled thermal stress analysis method is used to simulate the generation and propagation of elastic waves. Based on the finite element model, the interlaced imaging technique is used to image the rail defects.

2.1 Interlaced imaging principle

Since laser ultrasonics is not sensitive to the width of the defect, the model of the rail tread scratch is imaged on the rail by using a model that simultaneously excites ultrasonic waves on both sides of the rail. The model of the excitation model is shown in Figure 1.Two lasers are placed on both sides of the rail tread to generate excitation at the same time, and the excitation and receiving points are on the same side, the laser 1 is excited, the detector receives the signal at the corresponding A position, the laser 2 is excited and the detector receives the signal at the corresponding B position ,The scanning direction is as shown in the figure. Since the two lasers are not on the same side and the scanning direction is different, the excitation mode is called interlaced excitation. By using this method for imaging, not only can excitation and reception be performed simultaneously, but also the ultrasonic signals can be simultaneously received. Moreover, the lasers on both sides are simultaneously excited, and not only one-dimensional signal data can be obtained but also two-dimensional B-scan imaging can be obtained, which can solve the problem that the laser ultrasound is insensitive to the defect width and can quickly obtain the detected image and effectively display the defect feature.

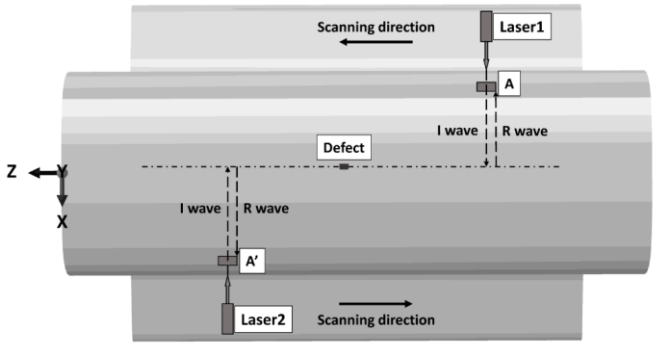

Figure 1 Interlaced laser detection of rail defect model

During the laser interlaced scanning excitation process, data acquisition is performed by the same side excitation same side receiving method, and after the alternate scanning, the obtained signal data with the defect information is obtained. Due to the unevenness of the rail tread and the mode conversion caused by the ultrasonic encountering defects, there will inevitably be a lot of noise data in the obtained data, which will seriously affect the subsequent imaging results. Firstly, the obtained data with the defect information needs to be filtered, and the noise signal is filtered to obtain the signal data with obvious defect information. Firstly, the obtained data with the defect information needs to be filtered, and the noise signal is filtered to obtain the signal data with obvious defect information. The next step is to integrate the two sets of data. Since the two sets of data are not excited and received at the same location, the relationship between the speed, time and displacement of the ultrasonic propagation in the material can be used to match the two sets of data. Finally, the two sets of data are integrated into a complete defect image.

2.2 Laser ultrasonic generation based on thermoelastic mechanism

When the power density of the laser incident on the surface of the material is lower than the energy threshold of the material, the thermoelastic effect plays an important role in the propagation of the ultrasonic wave. When the laser is incident on the material, the absorption of energy can only occur in the surface layer, thereby causing the local temperature of the surface of the irradiated material to rise, and then rapidly expanding to generate tangential stress, thereby generating ultrasonic waves. Therefore, under the thermal bomb mechanism, the heat conduction equation is as follows:

$$\rho C\frac{\partial T}{\partial t}-\nabla(k\nabla T)=Q \tag{1}$$

$$(\lambda+\mu)\nabla(\nabla u_1)-\mu\nabla\times\nabla\times u_1-\rho\frac{\partial^2 u_1}{\partial t^2}=\alpha(3\lambda+2\mu)\nabla T \tag{2}$$

where T is the temperature rise in the metal, k is the thermal conduction coefficient, ρ is the density, C is the constant specific heat, Q is the heat source created by laser irradiation, α is the linear thermal expansion coefficient, λ and μ are the Lamé constants and μ_1 is the displacement vector due to the thermo-elastic effect.

2.3 Theoretical basis of finite element method

Using the finite element method to study the laser ultrasonic problem can effectively establish the relationship between the laser parameters and the excited ultrasonic characteristics. The finite element form of the linear thermoelastic coupling equation for isotropic materials can be expressed as:

$$\begin{cases}[S]\{T\}_n+[C_V]\{\dot{T}\}_n=\{q\}_n\\ [M]\{\ddot{d}\}_n+(\alpha[M]+\gamma[K])\{\dot{d}\}_n+[K]\{d\}_n=(\sum_e\int[B]^T[D]\beta(\{T\}-\{T_0\})dS)_n\end{cases} \tag{3}$$

In the formula, $[S]$ is represented as a heat conduction matrix, $[C_v]$ is represented as a heat capacity matrix, $\{q\}$ is represented as a heat source vector, $\{T\}$ and $\{\dot{T}\}$ are expressed as temperature and node temperature change rates, respectively, $[M]$ is represented as mass matrix, $[K]$ is represented as stiffness matrix, α and γ is a frequency-independent constant, $[B]$ is the strain matrix, $[D]$ is the material elastic matrix, β is the thermal-elastic coupling coefficient of the material, $\{T_0\}$ is the initial temperature inside the material, $\{d\}$ 、 $\{\dot{d}\}$ 和 $\{\ddot{d}\}$ represent the displacement、 velocity and acceleration, n is the number of steps in time increment.

The finite element method solves the equations with explicit and implicit solutions. Compared with the implicit solution, the explicit solution does not require an iterative process and does not require simultaneous equations, thus simplifying the problem. Therefore, an explicit solution method is used to solve the formula (3).

The equations of motion for the body are integrated using the explicit central-difference integration rule:

$$\begin{aligned}\{\dot{d}\}_n&=\frac{1}{2\Delta t}\left(\{d\}_{n+\Delta n}-\{d\}_{n-\Delta n}\right)\\ \{\ddot{d}\}_n&=\frac{1}{\Delta t^2}\left(\{d\}_{n+\Delta n}-2\{d\}_n+\{d\}_{n-\Delta n}\right)\end{aligned} \tag{4}$$

The heat transfer equations are integrated using the explicit forward-difference time integration rule:

$$\{T\}_{n+1}=\{T\}_n+\Delta t_{n+1}\{\dot{T}\}_n \tag{5}$$

Bringing the formulas (4) and (5) into the formula (3), by using the explicit coupling technique, the solution of the equation can be obtained simultaneously.

In this paper, the finite element software is used for simulation. The model adopts 60 rails commonly used in China as the research model. The cross-sectional dimensions of the rail are shown in Figure 2.

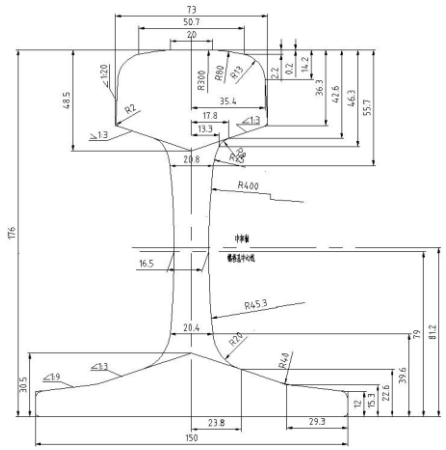

Figure 2 60 rail section size （*mm*）

When studying the influence of lateral width of laser spot on ultrasonic wave, the model of laser irradiation on rail tread surface is established, as shown in figure 3. The distance between excitation point and defect is $15mm$, and the distance between detection point and defect is $6mm$.

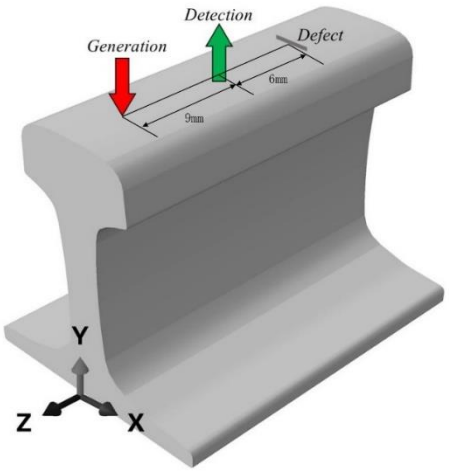

Figure 3 rail model

Table 1: The rail material performance parameters are shown.

Young's modulus	Poisson's ratio	density	Coefficient of thermal expansion
$210G\ Pa$	0.29	$7840kg \cdot m^{-3}$	$1.18\times10^{-5}K$

When using finite element software to analyze the rail model, the selection of mesh size and time step plays an important role in the stability and accuracy of the results. In general, the smaller time step, the more accurate showed the process of laser action on the rail, and the smaller the time step, the more accurate the solution, the more you can identify the high-frequency parts of the laser that produce ultrasonic waves. However, if the time step is too small, the computation time will be too long. Therefore, the time step of this paper is set as $\Delta t = 2\times10^{-9} m/s$, and the whole analysis time is set as $t = 1\times10^{-5} m/s$. In the whole model, the grid of the laser loading and transmission part is set as 1.5×10^{-4}, and other parts are set as 0.01.

When the laser is incident to the material surface, most of the energy is absorbed by the material, and some is reflected by the material. Domestic and foreign scholars regard the laser in the simulation as a pulse distributed in a Gaussian function in time and space, therefore, the laser energy density that the laser strikes the surface of the material and is absorbed by the material is:

$$Q = E_0 / (\tau \cdot A)(1-R) f(x,y) g(t) \tag{6}$$

Among them, $f(x,y)$ and $g(t)$ represent the laser pulse on the space and time distribution function:

$$f(x,y) = \exp^{(-\frac{(x-x_G)^2+(\alpha(y-y_G))^2}{R_G^2})} \tag{7}$$

$$g(t) = \frac{8t^3}{\tau^4}\exp(-\frac{2t^2}{\tau^2}) \tag{8}$$

In the formula, E_0 is the laser intensity of the laser incident on the surface of the material, τ is the pulse width of the laser pulse, A is the area of the laser source, R is the reflection coefficient of the material to the laser, and α is the ratio of the laser line source. When $\alpha = 1$, the laser source is a point source. When $\alpha \neq 1$, the laser source is a line source, (x_G, y_G) is the coordinate position of the laser incident center point, and R_G is the half width of the y-axis of the laser incident spot.

Laser incident on rail tread produces ultrasonic wave. When encountering defects, according to the Huygens principle, part of surface waves are reflected and return to the defect echo according to the original propagation route, part is transmitted to continue forward propagation, and some waves are converted into other modes. If there is no defect, the surface wave will continue to propagate forward, and the signal during the propagation is shown in figure 4. In the figure, sp is a sweeping longitudinal wave, R is a surface wave, and rR is a defect echo. It can be seen from Fig. 3 that the distance that the laser-induced ultrasonic wave encounters the defect return wave reaches the acceptance point is $21mm$, and the theoretical velocity of the surface wave in the steel rail is known to be $2996m/s$, according to the time formula of distance and speed, it can be calculated that the time to receive the defect echo at the acceptance point should be $7.01m/s$. As can be seen from Fig. 3, the time of arrival of the defect is $7.05m/s$, which is close to the calculated time, and the error is 0.57%. Therefore, the theoretical analysis of the model is correct.

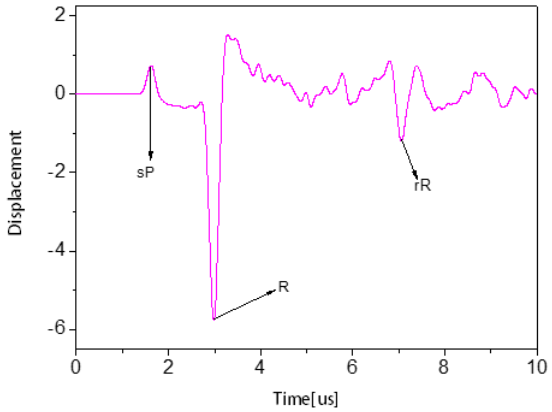

Figure 4 Surface wave signal

3. RESULTS

The simulation is carried out according to the model in Fig. 1. During the detection process, the data acquisition is performed by the same side excitation on the same side, and the scanning interval is $0.1mm$ and the scanning distance is $25mm$. After the alternating scanning, two sets of data are obtained, according to $s = v \cdot t$, the time coordinate can be changed to the position coordinate, and the imaging on both sides of the defect can be obtained separately, and then the image fusion is performed, and the two sides are image-fused into a complete defect imaging. According to the actual defect shape of the rail as shown in Fig. 5, the rail defect model is established as shown in Fig. 6, the defect width is $1.24mm$, and the depth is $0.5mm$. Because the 3D model takes a long time and the detection effect is poor, this paper

uses the 2D model to simulate. The two-dimensional simulation model is shown in Fig. 7. A is the position of the defect, B is the position of the signal detector, and *laser* is the excitation position of the laser source. The most dense part of the 2D model mesh is 3.2×10^{-5} , the analysis step is $2\times10^{-9}s$, and the total length of analysis is $3.2\times10^{-5}s$, and the parallel scanning operation takes 1 hour.

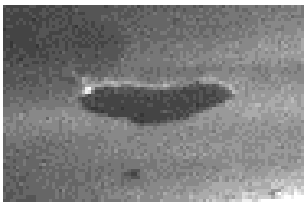

Figure 5 Actual tread defects of the rail

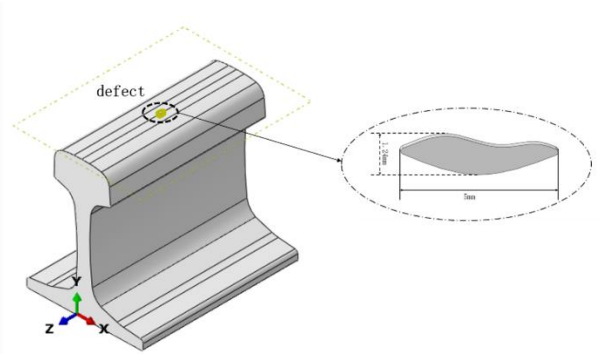

Figure 6 finite element model of rail tread detected by laser

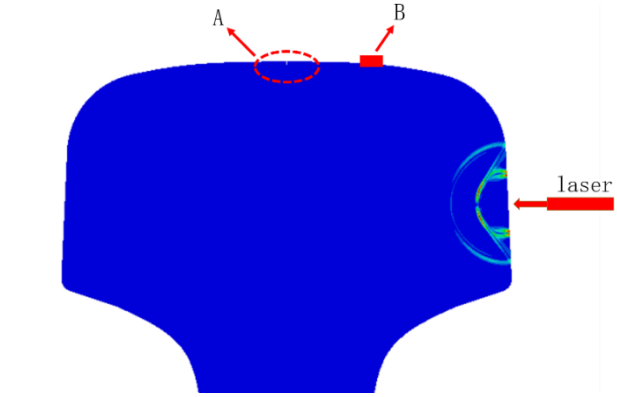

Figure 7 Equivalent two-dimensional model of laser-irradiated rail

The data obtained by the lasers 1, 2 are imaged as shown in Fig. 8. It can be seen from the figure that the defect shape on the side close to the laser can be clearly obtained, and the defect information on the other side is missing. It can be verified that laser ultrasound is not sensitive to the width of the defect.

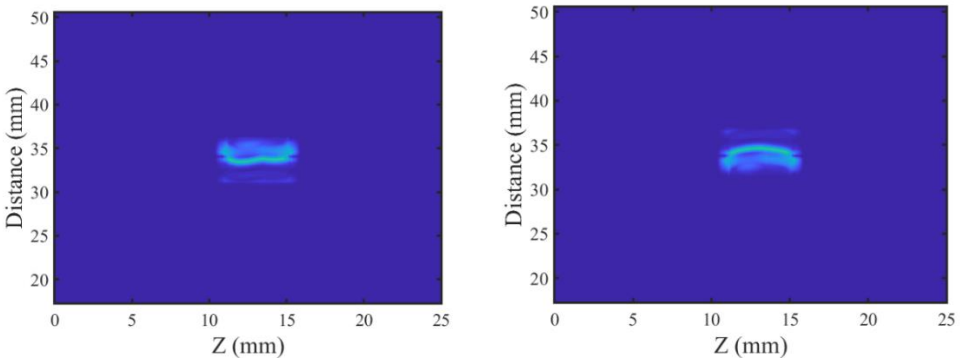

(a) Defect imaging of laser 1 (b) Defect imaging of laser 2

Figure 8 Single laser defect imaging

Image fusion technology is used to fuse the defect information on both sides to obtain the complete defect size and position information, as shown in Figure 9.

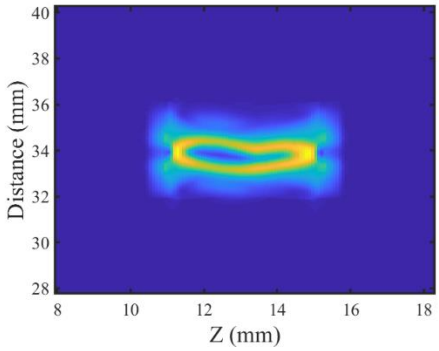

Figure 9 defect registration imaging

To study the amplitude of ultrasonic wave, use the previously mentioned model shown in figure 3. During the simulation, the laser pulse width is set to $5ns$, the laser energy is set to $100mJ$, and the lateral length is $10mm$. When the lateral width of the laser is changed to $2mm$, $1.5mm$, $1mm$, $0.5mm$, respectively, the received ultrasonic signal is observed. The ultrasonic signals received by the receiving point are shown in figure 10.

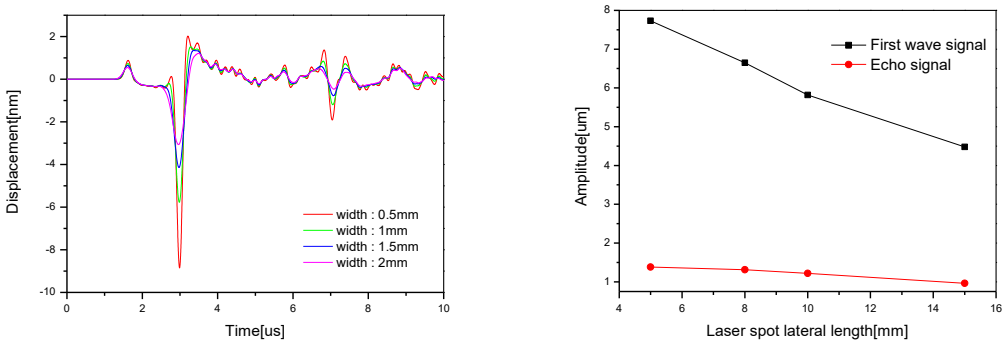

Figure 10 Ultrasonic signals and amplitudes received at different laser lateral widths

It can be seen from the above figure that the lateral width of the laser spot is inversely proportional to the amplitude of the ultrasonic wave. The smaller the width, the larger the amplitude of the ultrasonic wave excited by the laser, and the larger the amplitude of the defect echo, the easier it is to detect an accurate defect.

The lateral widths of the laser spots are changed to $0.5mm$ 、 $1mm$ 、 $2mm$, and the defects are imaged by the above-described interlaced imaging method as shown in figure 11.

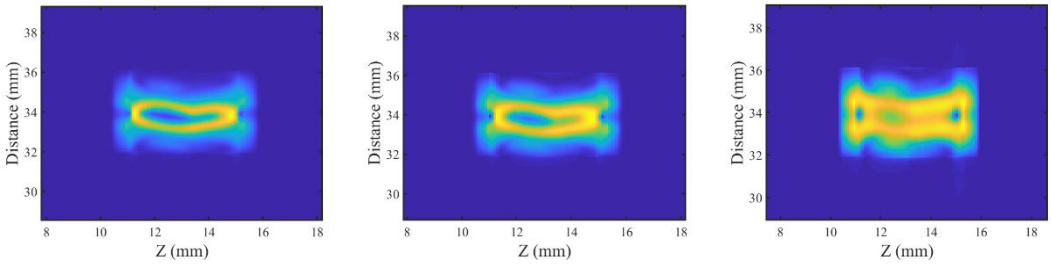

(a) registration defect imaging with laser spot lateral width set to $0.5mm$

(b) registration defect imaging with laser spot lateral width set to $1mm$

(c) registration defect imaging with laser spot lateral width set to $2mm$

Figure 11 Defect Imaging

As can be seen from Fig. 11, the lateral widths of the laser spots incident on the surface of the material are different, and the results of the interlaced imaging obtained are also different. When the spot width is $0.5mm$, the resulting image shape is close to the defect shown in Fig. 5, and the spot width is $1mm$, the obtained image shape is close to the defect shown in Fig. 6, however, the result is thicker than the line of the image with a spot width of $0.5mm$. When the spot width is $2mm$, the resulting image shape is much different from that of Figure 6. The original shape is not visible. It may be because the lines are thicker, causing the lines to coincide and the shape is distorted. From the above results, it can be concluded that the interlaced image is obtained. The technology verifies that changing the lateral size of the laser spot affects the detection of defects. The smaller the spot size, the finer the line of defects, and the closer the resulting defect shape is to the true shape shown in Figure 6.

4. CONCLUSION

In this paper, the interlaced laser imaging technology is studied, and the finite element model of ultrasonic wave irradiation on the surface of the rail is established. By changing the lateral width of the laser spot, the ultrasonic wave generated by the laser is changed, and the smaller the lateral width of the laser spot is, the easier it is to detect the defect. Using the interlaced laser detection of the rail defect model established in this paper, two lasers are used to generate ultrasonic detection defects by interleaving the two sides of the rail, and the data fusion method is used to image the defects, which solves the problem that the laser ultrasound is insensitive to the defect width, and can quickly detect the defect shape and position. The proposed method provides a reference for further establishing the actual rail inspection system.

ACKNOWLEDGMENTS

This work was supported by National Nature Science Foundation of China (Grant No. 61771409) and we wish to acknowledge them for their support. The authors also thank Southwest Jiaotong University Photoelectric Engineering Institute for their kind support in the experiment.

REFERENCES

[1] D. Milkovic, G. Simic, Z. Jakovljevic, J. Tanaskovic, V. Lucanin, Wayside system for wheel–rail contact forces measurements, Measurment 46 (2013) 3308–3318.

[2] H. Molatefi, H. Mozafari, Analysis of new method for vertical load measurement in the barycenter of the rail web by using FEM, Measurement 46 (2013) 2313–2323.

[3] Yang J, Ume I C. Laser ultrasonic technique for evaluating solder bump defects in flip chip packages using modal and signal analysis methods[J]. Ultrasonics Ferroelectrics & Frequency Control IEEE Transactions on, 57(4):920-932(2010).
[4] Sanderson T, Ume C, Jarzynski J. Longitudinal wave generation in laser ultrasonics[J]. Ultrasonics, 35(8):553-561(1998).
[5] Rose L R F. Point-source representation for laser-generated ultra-sound[J]. Journal of the Acoustical Society of America, 75(3):723-732(1984).
[6] Pantano A, Cerniglia D. Simulation of laser generated ultrasound with application to defect detection[J]. Applied Physics A, 91(3):521-528(2008).
[7] Pantano A, Cerniglia D. Simulation of laser-generated ultrasonic wave propagation in solid media and air with application to NDE[J]. Applied Physics A, 98(98):327-336(2010).
[8] Hernandez-Valle F, Dutton B, Edwards R S. Laser ultrasonic characterisation of branched surface-breaking defects[J]. Ndt & E International, 68:113-119(2014).
[9] Liu P, Nazirah A W, Sohn H. Numerical simulation of damage detection using laser-generated ultrasound.[J]. Ultrasonics, 69:248-258(2016).
[10] D. Cerniglia, B.B. Djordjevic, V. Nigrelli, Quantitative subsurface defect detection in composite materials using a non-contact ultrasonic system, in: IEEE Ultrasonics Symposium, pp. 751–754(2001).
[11] C. Cosenza, D. Cerniglia, B.B. Djordjevic, Non-contact ultrasonic ispection of skin/core bond in honeycomb with Lamb waves, in: IEEE Ultrasonics Symposium, Monaco,(2002).
[12] S. Kenderian, B.B. Djordjevic Jr., R.E. Green, Laser-based and air-coupled ultrasound as noncontact and remote techniques for testing railroad tracks, Mater. Eval. 60 (1) (2002) 65–70.
[13] D. Cerniglia, S. Kenderian, B.B. Djordjevic, G. Garcia, R. Morgan, Laser e trasduttore di accoppiamento in aria per l'ispezione ultrasonica non a contattonel settore ferroviario, Conferenza AIPnD, Matera, Italy, (2002).
[14] S. Kenderian, D. Cerniglia, B.B. Djordjevic, G. Garcia, Laser-air hybrid ultrasonic technique for dynamic railroad inspection application, in: Proceedings of 16th WCNDT 2004 – World Conference on NDT.
[15] K. Gonzales, S. Kendarian, D. Carter, A Smith, R Morgan, Non-contact interrogation of railroad axles using laser-based ultrasonic inspection, proceedings of JRC2005, Pueblo, Colorado. Doi: 10.1109/RRCON.2005.186070.
[16] Cavuto A, Martarelli M, Pandarese G, et al. Train wheel diagnostics by laser ultrasonics[J]. Measurement, 80: 99-107(2016).
[17] Cavuto A , Martarelli M , Pandarese G , et al. Experimental investigation by laser ultrasonics for high speed train axle diagnostics[J]. Ultrasonics, 55(1):48-57(2014).
[18] Arnold W, Betz B, Hoffmann B. Efficient generation of surface acoustic waves by thermoelasticity[J]. Applied Physics Letters, 47(7):672-674(1985).
[19] Liu P, Jang J, Yang S, et al. Fatigue crack detection using dual laser induced nonlinear ultrasonic modulation[J]. Optics and Lasers in Engineering, 110: 420-430(2018).
[20] Yi D, Pei C, Liu T, et al. Inspection of cracks with focused angle beam laser ultrasonic wave[J]. Applied Acoustics, 145: 1-6(2019).